Article

JOURNAL OF COMPOSITE MATERIALS

Journal of Composite Materials
2017, Vol. 51(18) 2549–2563

DOI: 10.1177/0021998316674348
journals.sagepub.com/home/jcm
SAGE

Effects of shallow angle on static strength and fatigue life of multi-directional laminates for wind turbine blades

Sung Kyu Ha[1], Alvaro Gorostidi Martinez de Lece[2], Carlos Donazar Moriones[2], Carlos Alberto Cimini Junior[3] and Chengzhu Jin[1]

Abstract

The effects of the shallow angle on the static strength and the fatigue life of the multi-directional glass fiber-reinforced plastics for wind turbine blades were presented based on experimental results and predictions. The static tests and the tension–tension fatigue tests under cyclic fatigue loads with a stress ratio of 0.1 were performed on bi-axial (BX, $[\pm\theta]$), tri-axial 1 (TA, $[0/\pm\theta_2]$), and tri-axial 2 (TX, $[0_2/\pm\theta]$) laminates with ply angles θ of 25°, 35°, and 45°. A multiscale approach was applied to predict the static tensile and compressive strengths and the S–N curves of BX, TA, and TX laminates based on the constituents: fiber, matrix, and interface. Three ply-based failure criteria (Hashin, Puck, and Tsai–Wu) were also employed to predict the static strength and compare with the experimental results. The predictions and the experimental results show that the tensile strength increases as θ becomes shallower, while laminates with a shallow ply angle of 35° showed similar or even lower compressive strengths, especially for TA and TX laminates. The laminate fatigue life increases as θ becomes shallower. The shallow angle effect on strength and fatigue life is greater for BX than TA and TX laminates since the ply angle θ plays a more important role in BX. By using the multiscale approach, the shallow angle effect on the laminate static and fatigue behaviors were also explained based on the ply stresses as well as the constitutive micro stresses.

Keywords

Wind turbine blade, bi-axial and tri-axial laminates, shallow angle, fatigue life, multiscale approach

Introduction

Glass fiber-reinforced plastics (GFRP) have been widely used for wind turbine blades due to their high specific stiffness, high specific strength, and excellent long-term durability.[1] It is well known that bi-axial (BX, $[\pm\theta]_S$), tri-axial 1 (TA, $[0/\pm\theta_2]_S$), and tri-axial 2 (TX, $[0_2/\pm\theta]_S$) laminates play an important role in the composite blades. As demand has increased for the development of large-scale wind turbine blades for the wind energy market, weight reduction of the blade has become one of the most critical issues.[2] One of the solutions is to apply various combinations of conventional 45° oriented plies and non-conventional plies oriented at shallows angles of 35° and 25°. Hayat et al.[3] studied the mass reduction of a 5MW wind turbine blade with symmetric and asymmetric skins using combinations of conventional 45° and shallow angles such as 25° and −5°. By using shallow angled skins, a thinner spar cap was designed, and the total blade mass was reduced up to 14%, meeting the design requirements.

A large number of studies have been conducted to observe the effect of the fiber orientation on the static and fatigue behaviors of the multi-directional laminates. Rotem and Hashin[4] performed experiments on BX with different fiber angles for comparison with

[1]Department of Mechanical Engineering, Hanyang University, Korea
[2]Acciona Windpower S.A., Avda Ciudad de la Innovación 3, Spain
[3]Department of Structural Engineering, Federal University of Minas Gerais, Brazil

Corresponding author:
Sung Kyu Ha, Hanyang University, 222 Wangsimni-ro, Seongdong-gu, Seoul 04763, Republic of Korea.
Email: sungkha@gmail.com

their proposed fatigue theory. Laminates with various fiber angles of 30°, 35°, 41°, 45°, 49°, 55°, and 60° were considered under the static tensile loading and the pure tension fatigue loading with a stress ratio (R) of 0.1. The fatigue behavior of BX with six fiber orientations and four different widths for $R = 0.05$ was presented by Kujawski.[5] Plenty of experiments on [θ] laminates with six different θ under static tensile and compressive loadings as well as fatigue loadings of seven different R-values have been performed by Kawai et al.[6] to propose an anisomorphic constant life diagram (CLD) of carbon/epoxy laminates. Philippidis and Vassilopoulos[7] studied the effect of the fiber direction on the fatigue life of the laminates under tension–compression ($R = -1$) loadings. Laminates with lay-up sequences of $[0/(\pm 45)_2/0]$ were selected, and four different types of off-axis loading directions were considered to observe the stiffness degradation for different off-axis angles. Studies on the cross-ply laminates ([0/90]) with different fatigue loading orientations were also presented previously.[8,9] The composite technologies research group at Montana State University has been working on the fatigue behavior of fiber-reinforced plastics for the wind turbine blades previously.[10,11] It has been observed that the fiber off-axis angles of the laminates are mostly the conventional 45°, and no other fiber angle has been studied by the Montana State University group.

A variety of methodologies have been used to predict the static and the fatigue behaviors of the composite laminates. The ply-based failure criteria (FC) such as the Tsai and Wu,[12] Hashin,[13] and Puck[14] FC, have been widely used to predict the laminate static strengths. Philippidis and Passipoularidis[15] observed the probabilistic distribution of the laminate residual strength after fatigue, and proposed phenomenological theories. Considerable amount of experimental efforts were included to better predict the test data. Kawai et al.[16–20] proposed an anisomorphic CLD based on experimental results, which can predict the fatigue lives of various laminates for different stress ratios, temperatures, and fiber orientations. However, it was shown that a lot of experimental data should be needed to construct the anisomorphic CLD. Miyano et al.[21–28] proposed a fatigue life prediction approach named accelerated testing methodology (ATM), by applying the time-temperature superposition principle (TTSP), which is originally for temperature-dependent elastic properties of linear viscoelastic materials, to static, creep, and fatigue strengths of both polymeric matrix and associated composites.

Most of above-mentioned conventional approaches for predicting laminate strength and fatigue are either ply- or laminate-based. It was shown that these models require a lot of tests and complicated theories to determine the parameters which are costly in both money and time. Recently, micromechanics of failure (MMF) was proposed by Ha et al.[29] and Huang et al.[30] which are based on the actual building block of composites, i.e. fiber, matrix, and interface. This simple and generic theory presented reasonable predictions compared with the experimental results and the widely used ply-based FC. Later on, a multiscale-based fatigue life prediction methodology called MMFatigue was proposed.[31,32] As an extension of MMF, MMFatigue includes theories of the micromechanics and the constituent fatigue models. Therefore, MMFatigue is able to predict individual constituent fatigue failure in each ply in order to predict the fatigue behavior of the laminate, and the comparison between prediction and test data of various laminates showed satisfactory agreement. MMF and MMFatigue, which are multiscale-based approaches, provide the effective methodologies to predict the laminate mechanical behavior by minimizing the number of required experiments for determining parameters.

As the design of light large-scale blades using shallow angled laminates draws an increasing amount of attention, it has become necessary to have a comprehensive summary of the effects of shallow angles on the mechanical behavior of the bi-axial and tri-axial laminates. This paper presents the effects of shallow angles on the static strengths and the fatigue lives of the bi-axial and tri-axial laminates based on predictions and test results. The static tensile and compressive tests were performed for BXθ, TAθ, and TXθ laminates with three different values of θ: the conventional 45° as well as shallow angles of 35° and 25°. The tension–tension fatigue tests under the cyclic fatigue loads with a stress ratio of 0.1 were performed to measure the S–N curves. A multiscale approach[29–32] was applied to predict the static strengths and the S–N curves of BX, TA, and TX laminates. Three ply-based FC, the Hashin, Puck, and Tsai–Wu, were also employed to predict the static strength in order to compare with the experimental results. Based on the multiscale approach, the shallow angle effects on laminate strengths and fatigue lives were explained in terms of the ply stresses and the constitutive stresses.

Methods

Strength prediction using ply-based failure criteria

In order to predict the laminate static strength, three commonly used ply-based failure criteria, the Tsai–Wu, Hashin, and Puck, were employed in combination with progressive damage models. By using these FC, the damage initiation for each ply was evaluated and the laminate strength was predicted using the first ply failure (FPF). The progressive damage models were used to degrade the damaged ply stiffness to predict the laminate strength based on the last ply failure

(LPF). The commercial finite element analysis (FEA) tool Abaqus[33] was employed for the static strength prediction using the Hashin FC and the energy dissipation-based progressive damage model. The Tsai–Wu and Puck FC were implemented using Microsoft Excel software. After the first ply failure initiation based on Tsai–Wu and Puck, it was assumed that the failed ply stiffness and Poisson's ratio were decreased to 10% of the original intact values to perform the progressive failure of the laminates. The predicted results were also compared with the test data to verify the accuracy of the failure criteria and the progressive damage models.

Multiscale approach for static strength prediction: MMF

A micromechanics-based multiscale approach named MMF[29,30] is applied to predict the laminate static strength based its three constituents: fiber, matrix, and interface.

Micromechanics to calculate constituent micro stresses. In order to calculate the micro stresses from the macro stresses applied to the ply, three regular arrays of micromechanical unit cell models were introduced in MMF

$$\boldsymbol{\sigma} = \mathbf{M}\bar{\boldsymbol{\sigma}} + \mathbf{A}\Delta\mathrm{T} \tag{1}$$

where $\boldsymbol{\sigma}$, $\bar{\boldsymbol{\sigma}}$, and ΔT represent the tensorial form of the micro stresses, macro stresses, temperature increments, respectively. The $\mathbf{M}$ (6×6 matrix) is called the stress amplification factor (SAF) for the macro stresses and $\mathbf{A}$ (6×1 matrix) is the stress amplification factor for the temperature increment. In this paper, the hexagonal unit cell model was used since it shows the most reasonable micro stress distributions comparing to the random fiber arrays.[34]

Failure criterion for each constituent. After the micro stresses were calculated, the constitutive failure criteria were applied to predict the failure of each constituent. For fiber, a maximum longitudinal stress failure criterion was employed

$$\sigma_{f1} \geq \mathrm{T_f} \quad \mathrm{OR} \quad \sigma_{f1} \leq -\mathrm{C_f} \tag{2}$$

where $\mathrm{T_f}$ and $\mathrm{C_f}$ are fiber longitudinal tensile and compressive strength, respectively, and σ_{f1} is the micro stress component in the fiber along the longitudinal direction.

For the matrix, the Stassi failure criterion[35] was used

$$\frac{\sigma_{\mathrm{VM}}^2}{\mathrm{C_m T_m}} + \left(\frac{1}{\mathrm{T_m}} - \frac{1}{\mathrm{C_m}}\right)\mathrm{I_1} \geq 1 \tag{3}$$

where σ_{VM} and $\mathrm{I_1}$ are the von Mises equivalent stress and the first stress invariant of the micro stresses at a point within the matrix, respectively. $\mathrm{T_m}$ and $\mathrm{C_m}$ denote the tensile and compressive strengths of matrix, respectively.

For the interface, a quadractic failure criterion was used in MMF

$$\left(\frac{\langle\sigma_n\rangle}{\mathrm{Y_n}}\right)^2 + \left(\frac{\tau}{\mathrm{Y_s}}\right)^2 \geq 1 \tag{4}$$

where σ_n, τ, $\mathrm{Y_n}$, and $\mathrm{Y_s}$ are interfacial normal traction, shear traction, normal strength, and shear strength, respectively. The Macauley brackets '$< >$' mean that normal stress will contribute to failure only when it is positive.

Laminate strength prediction based on first constituent failure and last constituent failure. By using the constituent failure criteria, the constitutive failure can be predicted and the laminate strength can be estimated based on the first constituent failure (FCF). After FCF, the failed constituent stiffnesses are degraded and the ply and laminate stiffnesses are also degraded accordingly. The ply stresses and the micro stresses are then redistributed causing further constituent failure, and the laminate strength can be predicted based on last constituent failure (LCF).

Multiscale approach for fatigue life prediction: MMFatigue

As the extension of MMF, MMFatigue[31] includes theories of the micromechanics and the constitutive fatigue models to predict the fatigue damage of each constituent, and the damage accumulations as well as the progressive failure to predict the laminate fatigue life.

Equivalent stress model for multi-axial stresses. The equivalent stress models are introduced to replace the multiaxial time-varying micro stresses by one equivalent stress component. For fiber, the longitudinal stress component is taken as the equivalent stress

$$\sigma_{\mathrm{eq,f}}(\mathrm{t}) = \sigma_{\mathrm{f1}}(\mathrm{t}) \tag{5}$$

In case of matrix, the equivalent mean stress and the stress amplitude are derived from equation (3), with some modifications such that the equivalent stresses are equal to the actual stress components under the uniaxial loading case[32]

$$\sigma_{\mathrm{eq}}^{\mathrm{mean}} = \mathrm{sgn}\left(\mathrm{I_1^{mean}}\right)\frac{\left\{\begin{array}{c}(\beta-1)\left|\mathrm{I_1^{mean}}\right| \\ +\sqrt{(\beta-1)^2\left(\mathrm{I_1^{mean}}\right)^2+4\beta\left(\sigma_{\mathrm{VM}}^{\mathrm{mean}}\right)^2}\end{array}\right\}}{2\beta}$$

$$\sigma_{eq}^{amp} = \frac{(\beta-1)I_1^{amp} + \sqrt{(\beta-1)^2\left(I_1^{amp}\right)^2 + 4\beta\left(\sigma_{VM}^{amp}\right)^2}}{2\beta} \quad (6)$$

where

$$\mathrm{sgn}\left(I_1^{mean}\right) = \begin{cases} 1 & \left(I_1^{mean} \geq 0\right) \\ -1 & \left(I_1^{mean} < 0\right) \end{cases} \quad (7)$$

Here, β is the ratio between C_m and T_m.
For interface, a critical plane model is applied

$$\sigma_{eq,i}(t) = \mathrm{sgn}(\langle\sigma_n\rangle, \tau)\sqrt{\langle\sigma_n\rangle^2 + (k_i\tau)^2} \quad (8)$$

where the function $\mathrm{sgn}(<\sigma_n>, \tau)$ is the sign of the one component between $<\sigma_n>$ and τ which has the greater absolute value. The material constant k_i is generally taken as the ratio of fatigue limit under completely reserved bending and torsional S–N curves. In MMFatigue, it is assumed that k_i is the ratio of Y_n and Y_s.

Constant life diagram for mean stress effect. After obtaining the equivalent mean stress and the stress amplitude, the effective stress is introduced to consider the mean stress effect. A constant life diagram (CLD) model considering the creep effect is proposed for each constituent[36,37]

$$\begin{cases} \sigma_{eff} = \dfrac{2T_c(T,t_f)\sigma_{amp}}{\left\{\begin{array}{l}[T_c(T,t_f) + C_c(T,t_f)] \\ -\left|2\sigma_{mean} - [T_c(T,t_f) - C_c(T,t_f)]\right|\end{array}\right\}} \\ \sigma_{eff} = b(T)N_f^{-\frac{1}{m(T)}} \end{cases} \quad (9)$$

where σ_{eff} is the effective stress including the effect of the mean stress. T_c and C_c represent the tensile and compressive creep strengths, which are function the temperature T and the time to failure t_f. Specially, in case of the interface, T_c denotes interfacial normal creep strength $Y_{n,c}$, and C_c denotes the shear creep strength $Y_{s,c}$. N_f, b, and m are the number of cycles to failure, and the magnitude and slope parameters of the effective S–N curve, respectively. The kinetic theory of fracture is used in MMFatigue to calculate the creep strength of the CLD model

$$t_f = \frac{h}{kT}\exp\left(\frac{U - \gamma T_c}{kT}\right) \quad (10)$$

where h, k, U, and γ are Planck constant, Boltzmann constant, activation energy, and activation volume of the material, respectively.

Based on the CLD and the kinetic theory, the constitutive fatigue life N_f can be predicted using the effective S–N curve measured from the experiment.

Fatigue damage accumulation and progressive failure. After calculating the N_f for each constituent, the accumulated damage was then calculated by using the Miner's rule

$$D = \sum_j \frac{n_j}{N_{f,j}} \quad (11)$$

where n_j and $N_{f,j}$ are the number of cycles applied and the number of cycles to failure under j-th loading, respectively. When D reaches 1, the constituent failure occurs and the laminate fatigue life is estimated based on the FCF. After FCF, similarly to the method used in MMF, the stiffness degradation of the constituent, ply, and laminate is performed and the final fatigue failure of the laminate is achieved when the laminate stiffness degradation reaches 50%,[38,39] and the fatigue life can be predicted based on LCF.

Experiment

Materials

Three types of the non-crimp fabric (NCF) laminates are used in this study: bi-axial (BX, $[\pm\theta]$), tri-axial 1 (TA, $[0/\pm\theta_2]$), and tri-axial 2 (TX, $[0_2/\pm\theta]$) with values of $\theta = 25^\circ$, 35°, and 45°. It is noticed that the TA has only 20% of 0° ply while TX has 50% of 0° ply in terms of the volume fraction. The BX and TX NCFs have an areal weight of 1200 g/m^2, and the TA NCF has an areal weight of 750 g/m^2, all provided by the Chomarat Group, with the Advantex E-glass fiber with the sizing of SE1500 from 3B Company. An epoxy resin system from Momentive Specialty Chemicals EPIKOTE^{TM} was used: resin MGS® RIMR 135 and curing agent MGS® RIMH 137 in a mixing ratio of 100:30 by weight.

Specimen fabrications and test methods

All of the NCF composite panels were fabricated using vacuum assisted resin infusion. The specimen fabrication procedures are explained in Figure 1. A wood plate with dimensions of 500 mm × 500 mm with fine outer surfaces was used as a base tool for the infusion process. The release agent was applied to the top of the clean base plate and allowed to dry for half hour. Double-backed vacuum tape was applied near the edges of the base plate. One peel ply, the NCF

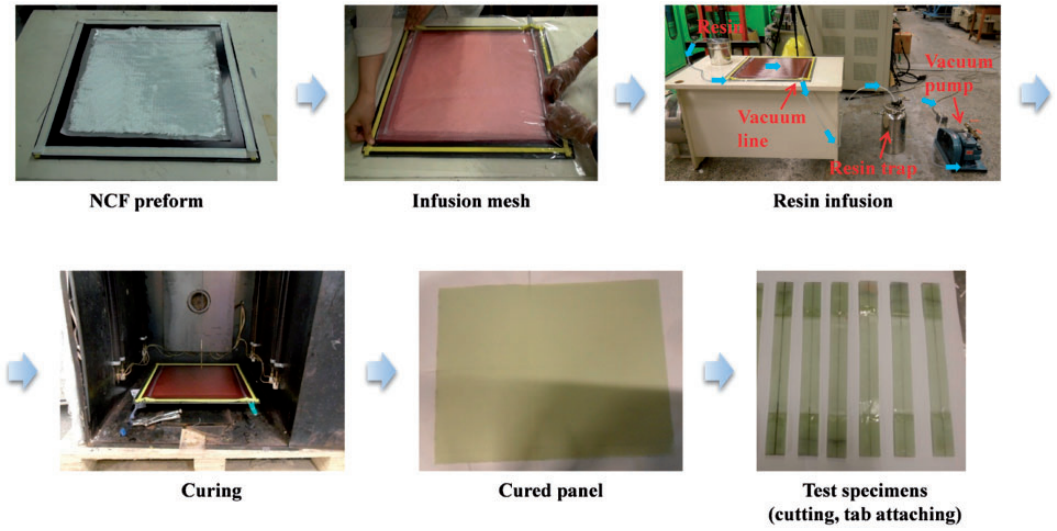

Figure 1. Specimen fabrication using resin infusion.

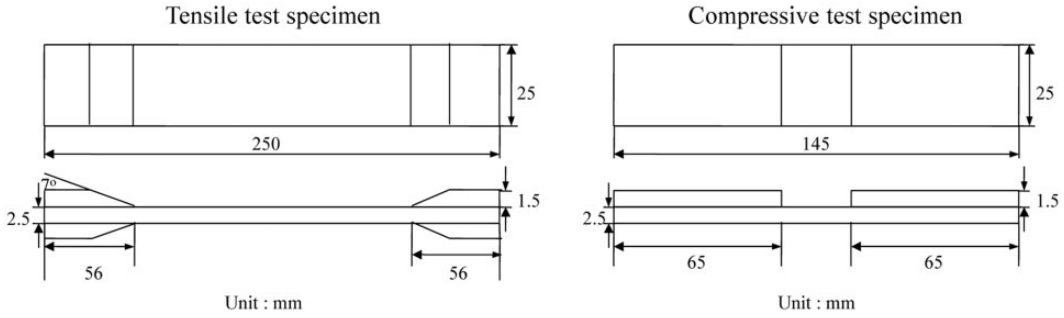

Figure 2. Dimensions of test specimens.

preforms, another one peel ply, and one resin infusion mesh were then placed in sequence. Inlet and outlet connectors and spiral tubes were placed at specific locations, and a vacuum bag was then attached to the whole infusion setup. The inlet and outlet vacuum tubes were connected to the vacuum pump to create a vacuum of –0.9 bar. After mixing the resin system according to the mixing ratio, it was degassed in a vacuum chamber at a vacuum of –1.0 bar in order to remove the air bubbles, and then the infusion was carried out. The resin trap was used as a reservoir for extra resin that came out with the air bubbles from the base plate. After the infusion, the base plate was placed in the curing oven for 18 h at 60°C. The cured composite panel was then cut into small panels using a diamond saw cutter. The tabs were then attached to the panels and then the specimens were cut. The edges of the test specimens were polished using sandpaper. The dimensions of the test specimens are shown in Figure 2. The fiber volume fraction was (V_f) measured based on the ASTM D792,[40] and range of V_f was 0.48 to 0.53.

Static tensile tests were performed according to ASTM D3039.[41] The in-house developed multifunctional horizontal electro-serve test machines were used for the tensile tests. A constant speed of 1 mm/min was applied to the composite specimens. Static compressive tests were performed based on ASTM D3410.[42] An MTS Landmark™ 370.10 servo-hydraulic test machine was used for static compressive tests. A constant speed of −1 mm/min was applied to the composite specimens. The fatigue tests were performed based on ASTM D3479.[43] T–T fatigue loadings with $R = 0.1$ and frequency = 1 Hz were applied in the fatigue tests. All the tests were run at room temperature, which is approximately 25°C.

Table 1. Ply properties for laminate strength prediction.

Type	Explanation	Symbol	Value
Stiffness and Poisson's ratio	longitudinal	E_x	40.0 GPa
	transverse	E_y	10.1 GPa
	shear	E_s	3.1 GPa
	Poisson's ratio	v_{xy}	0.27
Strength	longitudinal tensile	X	901.3 MPa
	longitudinal compressive	X'	656.6 MPa
	transverse tensile	Y	50.3 MPa
	transverse compressive	Y'	126.2 MPa
	shear	S	57.5 MPa
Puck failure criterion	fiber stiffness	E_{f1}	82 GPa
	fiber Poisson's ratio	v_{f12}	0.3
	stress magnification factor	$m_{\sigma f}$	1.3
	slope of the fracture envelope for normal stress>0 at normal stress = 0	$P_{\perp\parallel}^{(+)}$	0.3
	slope of the fracture envelope for normal stress<0 at normal stress = 0	$P_{\perp\parallel}^{(-)}$	0.25
Hashin progressive damage model	longitudinal tensile fracture energy	G_{ft}	1.1E7 J
	longitudinal compressive fracture energy	G_{fc}	5.9E6 J
	transverse tensile fracture energy	G_{mt}	1.4E5 J
	transverse compressive fracture energy	G_{mc}	8.7E5 J

Table 2. Constitutive properties for laminate strength and life predictions.

		Constituent properties		
Explanation	Symbol	Fiber	Matrix	Interface
Young's modulus	E (GPa)	74	3.0	–
Shear modulus	G (GPa)	30.8	1.24	–
Poisson's ratio	v (–)	0.2	0.35	–
Tensile strength	T (MPa)	1890	68.3	–
Compression strength	C (MPa)	1280	85.6	–
Normal strength	Y_n (MPa)	–	–	110.5
Shear strength	Y_s (MPa)	–	–	62.7
S–N curve slope	m (–)	6.245	4.747	7.5
Fatigue strength	b_0 (MPa)	2758.1	186.1	159.2
Activation energy	U_0 (J)	1.16e-18	2.78e-19	2.65e-19
Activation volume	Υ (m^3)	5.49e-28	1.50e-27	2.01e-27

Results and discussions

Shallow angle effect on static strengths of BX, TA, TX

Variation of ply stresses with respect to ply angles. Table 1 presents the ply material properties used for the laminate strength prediction. These values were based on our own testing and test data provided by the 3B company. The parameters for the Puck failure criterion were referred to Puck and Schürmann,[14] and the parameters for the progressive damage model were determined based on Camanho and Dávila.[44]

Table 2 shows the constitutive properties for strength and life prediction of laminates using MMF and MMFatigue. Matrix properties were obtained based on the pure resin tests, and the fiber properties were indirectly measured from the composites previously.[32] The single fiber fragmentation test (SFFT)[45] was performed to measure the interfacial shear strength. The interfacial normal strength and the fatigue parameters were back-calculated from the composite laminates.

Before showing the results of the static strengths, the ply stresses with respect to the ply angles are studied, as shown in the Figures 3 to 5. Each ply stress is normalized by corresponding ply strength, and each ply strength is normalized by the longitudinal tensile strength (X). The reason of using the normalized ply stresses and the normalized ply strengths is to observe which stress component is critical to the ply failure.

The shear stress (σ_s) is dominant for BX, as shown in Figure 3. σ_s decreases when θ changes from 45° to 25°, which means that BX with a shallower angle is capable of supporting more tensile or compressive loads.

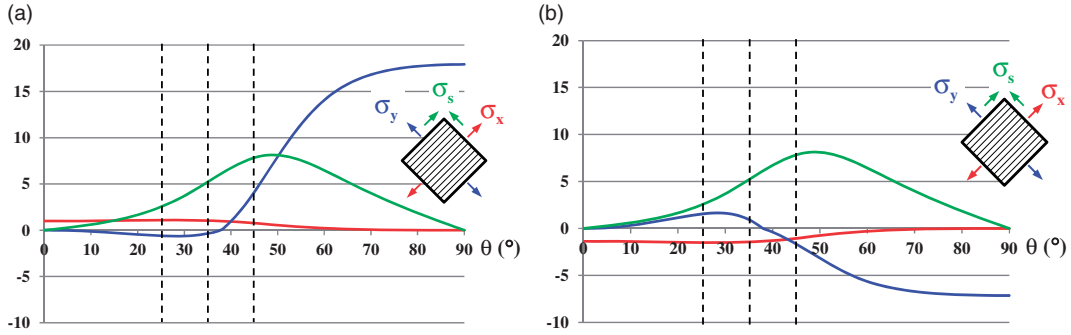

Figure 3. Normalized ply stresses of BX under (a) tension, (b) compression.

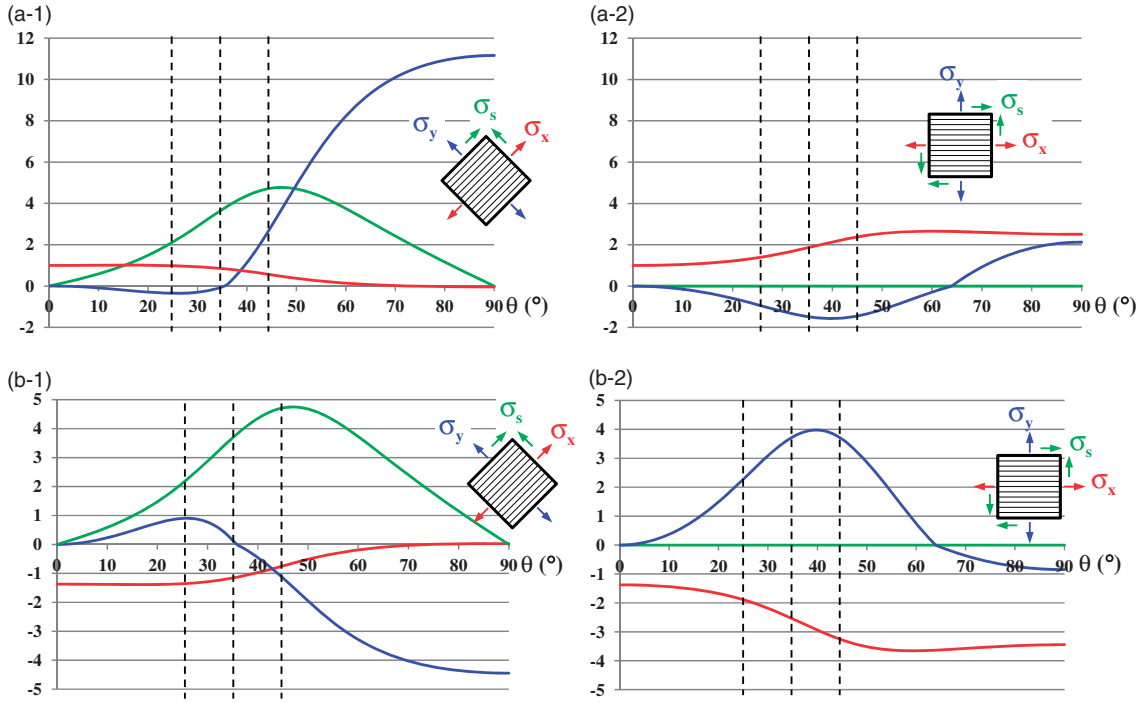

Figure 4. Normalized ply stresses of TA at (a-1) θ ply under tension, (a-2) 0° ply under tension, (b-1) θ ply under compression, and (b-2) 0° ply under compression.

In case of the TA and TX laminates, the variations of ply stresses at θ ply have similar trends as BX, as shown in Figures 4 and 5. At 0° ply, the longitudinal stress (σ_x) and the transverse stress (σ_y) are critical factors. Under the tensile loading, σ_x and σ_y decrease with the shallower angle when θ ranges between 25° and 45°. However, σ_x decreases but σ_y increases under the compressive loads. It is noted that the 0° ply is subject to transverse tensile load of which direction the ply strength is very low. It is observed in Figures 4(b-2) and 5(b-2) that σ_y at 0° is similar for $\theta = 35°$ and $\theta = 45°$. One of the reasons can be the effect of the θ on the Poisson's ratio (v_{12}) of the TA or TX laminate. As shown in the Figure 6, when θ is smaller than 65°, v_{12} is larger than the one when θ is equal to 0°, which indicates that v_{12} of the 0° ply is smaller than that of θ ply, such that 0° ply is forced to extend transversely. This requires a transverse tensile load to occur at 0° ply that is critical to 0° ply failure. It is found in the figure that v_{12} of TX35 is larger than that of TX45. Therefore, more transverse tensile stress will occur for 0° ply of TX35. A similar trend was also found in Hoppel and De Teresa.[46]

Shallow angle effect on static strengths of BX, TA, TX. The static tensile strengths X_T of BX, TA, and TX were

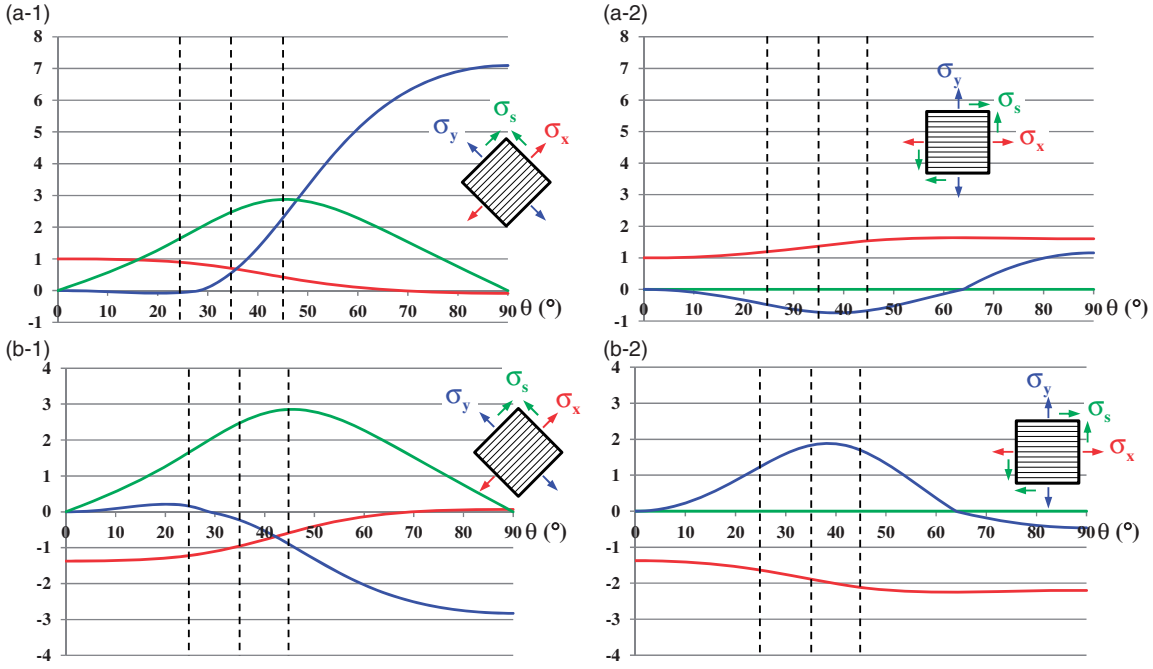

Figure 5. Normalized ply stresses of TX at (a-1) θ ply under tension, (a-2) 0° ply under tension load, (b-1) θ ply under compression, and (b-2) 0° ply under compression.

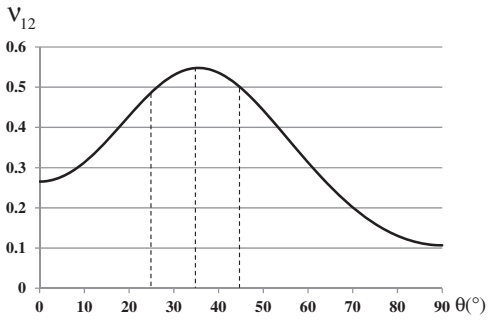

Figure 6. Poisson's ratio of TX laminate.

measured and predicted, as summarized in Figure 7. The dots represent the test data, and for the ply-based predictions, the dotted lines and the full lines represent the predictions according to the FPF and LPF, respectively. For the MMF predictions, the dotted lines and the full lines represent the predictions according to the FCF and the LCF, respectively.

For the BX laminates, the predicted X_T values based on the FPF (or FCF) and LPF (or LCF) are the same, while the X_T values of the TA or TX laminates based on the FPF (or FCF) and LPF (or LCF) are different. The difference between an FPF(or FCF)-based prediction and an LPF(or LCF)-based prediction becomes larger as the volume fraction of the 0° ply gets larger because more 0° plies are capable of withstanding more external loads after the initial failure of the angled plies.

Based on the predictions, the failure modes of the laminates can also be clarified. The ply-based predictions indicate that the FPF is due to θ ply and the LPF is due to 0° ply, and MMF predicts that FCF is due to interface or matrix at θ ply and LCF is due to fiber at 0° ply. Previously, it was observed in Figures 3 to 5 that at θ ply the shear stress is critical, and at 0° ply longitudinal stress is critical in the ply failure. It is well known that the ply shear stress causes the matrix or interface failure and the ply longitudinal stress relates the fiber failure. Therefore, the failure modes from ply-based predictions and MMF predictions coincide.

It is reasonable that the test results are closer to the LPF-based and LCF-based predictions, and they are in acceptable agreements. Both test results and predictions show a similar trend that shallower angles improve X_T significantly. For example, compared with the BX45 laminates, X_T can more than double for BX25, and more than 40% increase of X_T can be obtained when θ of 35° is used. In case of the TA laminates, X_T is increased by over 50% from TA45 to TA25 and by over 10% from TA45 to TA35. X_T of TX25 is about over 20% larger than that of TX45, and X_T of TX35 increases approximately 10% as compared to that of TX45. The increase in X_T is more obvious for BX than TA and TX, since there is no 0° ply in BX and the effect of the shallow angle is more critical.

The shallow angle effects on the static compressive strength X_C are shown in Figure 8. The failure modes of the laminates under the compression are

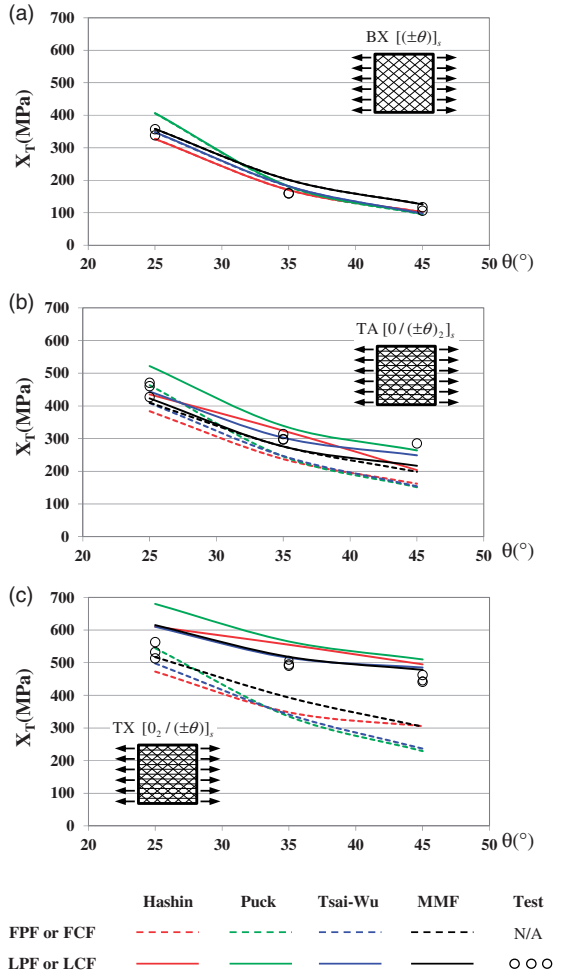

Figure 7. Static tensile strength: (a) BX, (b) TA, and (c) TX.

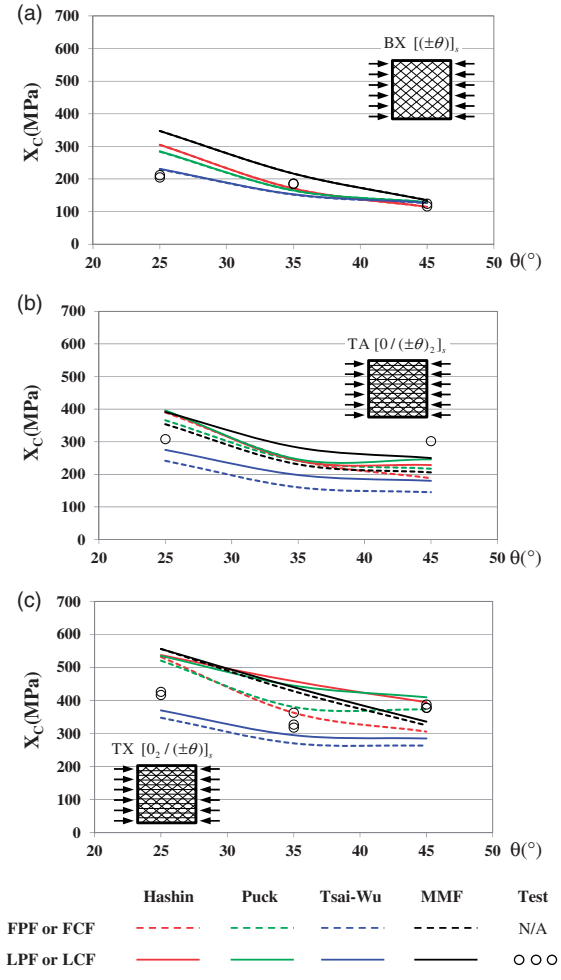

Figure 8. Static compressive strength: (a) BX, (b) TA, and (c) TX.

different from the case under the tensile loads. Tsai–Wu predict that the FPF is due to 0° ply, while Puck and Hahsin's predictions indicate that the FPF is due to θ ply. MMF predicts that FCF is due to interface or matrix at θ ply except for TX25 which FCF is due to fiber at 0° ply.

Compared with tensile strength, the shallow angle provides less effect on the compressive strength. Based on the test results, X_C of BX25 is over 70% larger than that of BX45, and BX35 has a 55% higher X_C than BX45. A similar trend is observed for TA and TX. For example, in the case of TX laminates, X_C is increased by 10% for a 25° angle as compared to 45°. No increase of X_C can be observed for TX when 35° is used. The test results show that X_C of TX35 is even lower than that of TX45. The same conclusion was found and the reasons are explained in Shirazi and Varvani-Farahani.[39] One of the main reasons is the Poission's effect producing transverse tensile stress at the 0° ply, as previously explained in Figure 6.

Shallow angle effect on fatigue life of BX, TA, TX

Shallow angle effect on S–N curves of BX, TA, TX. Figure 9 shows the S–N curves of BX, TA, and TX laminates. The fatigue stress is expressed in terms of the maximum stress σ_{max}, while the fatigue life is presented in terms of the number of cycles in log scale. The red, green, and blue corresponds to the results when θ is equal to 25°, 35°, and 45°, respectively. The dots represent the test results while the dotted and full lines represent the MMFatigue predictions based on FCF and LCF, respectively.

Generally, the predictions and the test results are in acceptable agreements in most cases, and they show similar trend that a shallower angle provides a longer laminate fatigue life under the tension–tension fatigue loads.

Similarly to the case of the static strength, the FCF-based and LCF-based predictions of the BX laminates are exactly the same because there is only $+\theta$ (or $-\theta$) ply. For TA laminates in case of TA35 and TA45, the

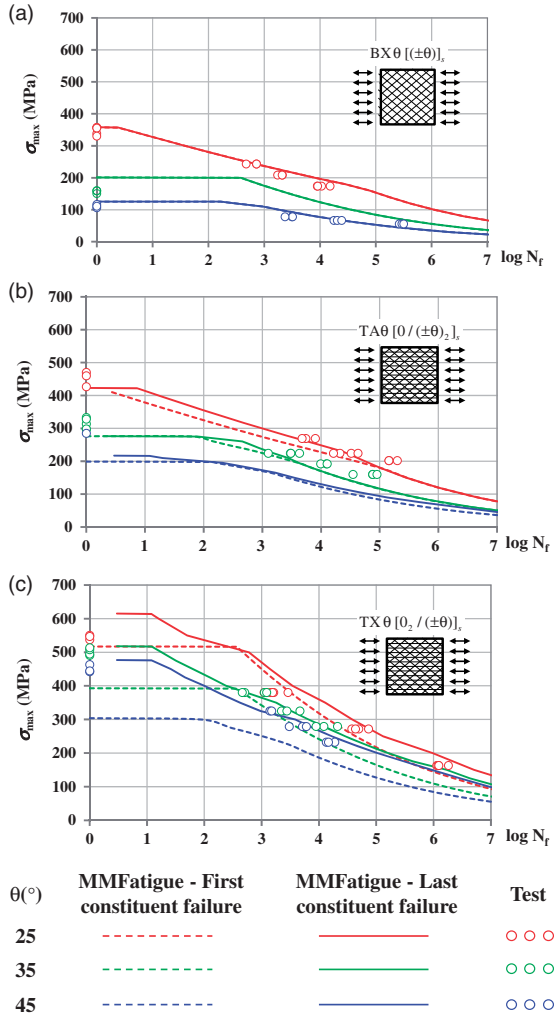

Figure 9. Shallow angle effect on S–N curves of (a) BX, (b) TA, and (c) TX.

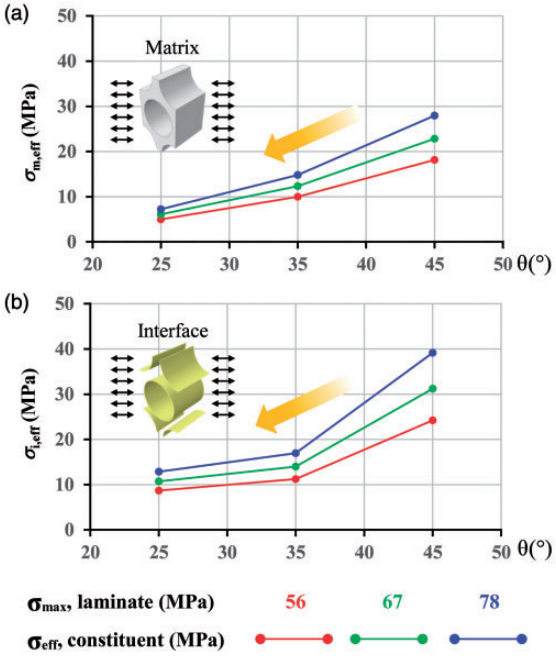

Figure 10. Shallow angle effect on constitutive effective stresses of BX at [θ] ply: (a) matrix, (b) interface.

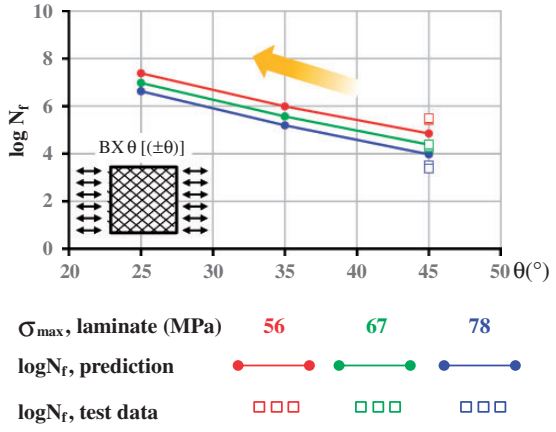

Figure 11. Shallow angle effect on fatigue life of BX under different fatigue loads.

FCF-based and LCF-based S–N curves are almost the same indicating that the 0° ply does not contribute to the laminate failure. This is because, based on the MMFatigue prediction, after the failure of θ ply, the laminate stiffness in the longitudinal direction is degraded enough to satisfy the failure prediction (i.e. laminate stiffness degradation is more than 50%) and no further progressive failure is necessary. However, a slight difference between FCF-based and LCF-based S–N curves were found for TA25 meaning that after the θ ply failure the 0° ply also contributes to the laminate failure. The difference between FCF-based and LCF-based predictions is mainly due to the fiber at the 0° ply, and it becomes more observable for TX laminate than for TA laminates due to the larger volume fraction of 0° ply.

The shallow angle effect on the laminate fatigue life is observed in Figure 9. Compared with the 45°, a shallow angle of 25° provides much longer fatigue life. For example, in case of the BX laminate, and when σ_{max} is 78 MPa, fatigue life of BX25 is 457 times of BX45, and σ_{max} is 56 MPa, fatigue life of BX25 is 339 times of BX45. For the TX laminate, due to the 50% volume fraction of the θ° ply, the shallow angle of 25° does not improve fatigue as much as the case of BX, but it still increases the fatigue life in a large amount compared with the 45°. For example, when σ_{max} is 325 MPa, fatigue life of TX25 is 25 times of TX45, and when σ_{max} is 232 MPa, fatigue life of TX25 is 9 times of TX45. Compared with the 25°, less improvements in the fatigue life were observed when $\theta = 35°$ is used. In case of

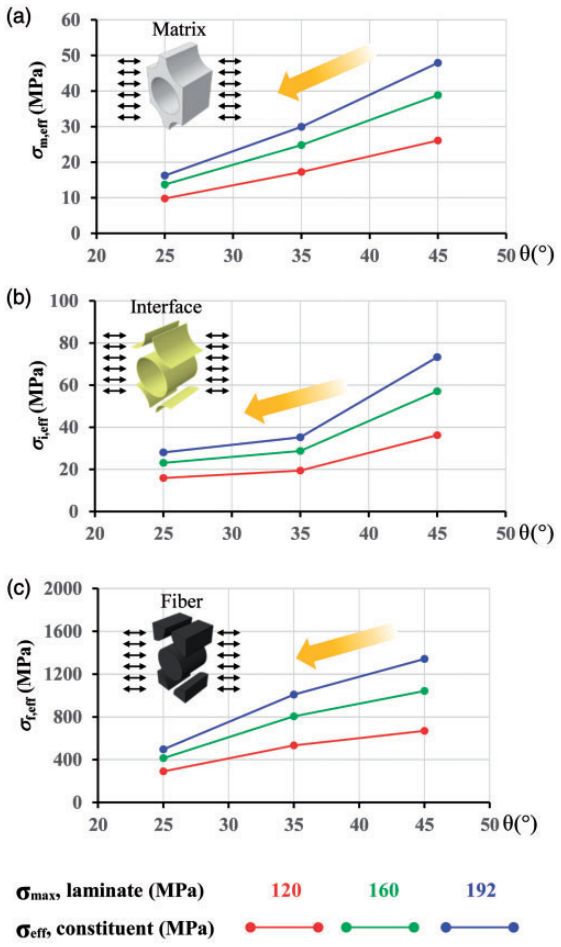

Figure 12. Shallow angle effect on constitutive effective stresses of TA at (a) matrix of [θ] ply before [θ] ply failure, (b) interface of [θ] ply before [θ] ply failure, and (c) fiber of [0] ply after [θ] ply failure.

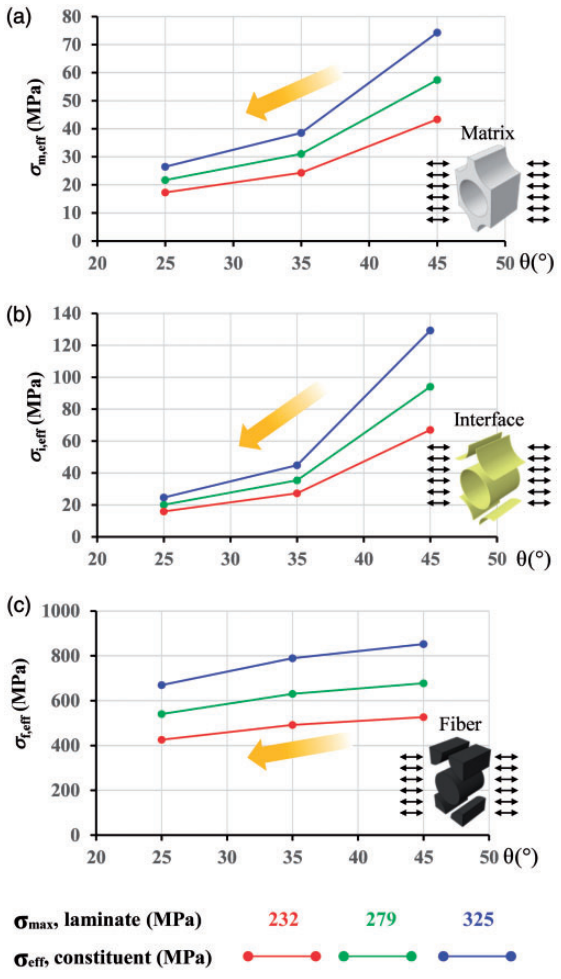

Figure 14. Shallow angle effect on constitutive effective stresses of TX at (a) matrix of [θ] ply before [θ] ply failure, (b) interface of [θ] ply before [θ] ply failure, and (c) fiber of [0] ply after [θ] ply failure.

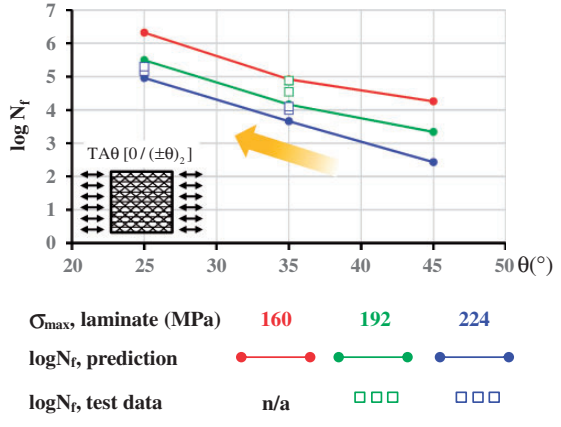

Figure 13. Shallow angle effect on fatigue life of TA under different fatigue loads.

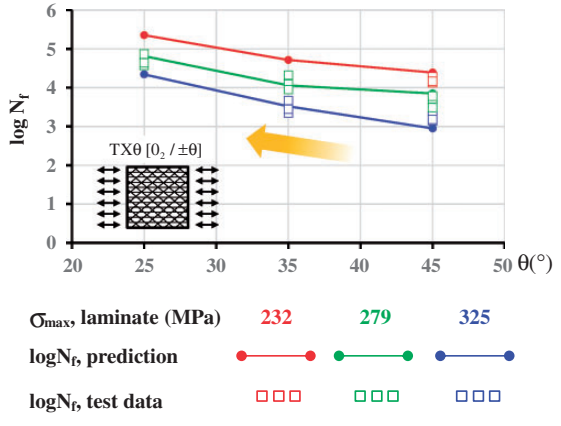

Figure 15. Shallow angle effect on fatigue life of TX under different fatigue loads.

the BX and the TA laminates, the failures are mainly due to θ ply, so it is important to understand the variation of matrix and interface stresses at θ ply with respect to θ. For TX, since the portion of 0° ply is 50%, it may be more important to observe the variation of the fiber stress at the 0° ply.

Explaining shallow angle effect on laminate fatigue life using constitutive effective stress. In order to explain the shallow angle effect of the laminates fatigue lives, the constitutive effective stresses were calculated. Three different fatigue load cases were selected for each BX, TA, and TX laminate, and the variation of the constitutive micro stresses and the laminate fatigue lives with respect to θ were plotted.

The effective stresses of the matrix ($\sigma_{m,eff}$) and interface ($\sigma_{i,eff}$) of BX laminates are shown in Figure 10. As θ becomes shallower, $\sigma_{m,eff}$ and $\sigma_{i,eff}$ decrease. Based on the calculated $\sigma_{m,eff}$ and $\sigma_{i,eff}$, the constitutive fatigue damages were determined and the laminate fatigue lives were predicted, as shown in Figure 11. Due to the decrease of constituent effective stresses, the BX fatigue life increases when θ becomes smaller.

The case of the TA laminates is more complicated than BX since there is the 0° ply except the θ ply. Considering that the fraction of θ ply is 80% and 0° ply is only 20%, the matrix or interface failure at θ ply is dominant while the fiber at the 0° ply may contribute to the failure of the TA laminate.

Figure 12 shows the constitutive effective stresses at the θ ply of the TA laminate, and the redistributed fiber effective stresses at the 0° ply after θ ply failure. Obvious decreases of micro stresses were observed as θ becomes shallower.

Figure 13 presents the fatigue life of the TA laminates under three different fatigue load level. Due to the less constituent effective stresses, TA with a shallower angle has a longer fatigue life.

In case of the TX laminate, since 0° ply possesses 50% volume fraction of the TX, the laminate failure is dominated by the failure of the fiber at 0° ply. The constitutive effective stresses under three different fatigue loads are shown in Figure 14. It is observed that the fiber stress decreases as θ becomes shallower causing a longer TX fatigue life. Compared with the case of BX and TA, shallow angle effect is less for TX.

Conclusions

The effects of shallow angles on static strengths and fatigue lives of BX ($[\pm\theta]_S$), TA($[0/\pm\theta_2]_S$) and TX ($[0_2/\pm\theta]_S$), which are typical laminates for wind turbine blades, were evaluated based on experiments and predictions.

Static tensile and compressive tests were performed to measure the laminate strengths, and tension–tension fatigue tests for $R = 0.1$ were performed to measure the S–N curves. Three ply-based failure criteria, the Hashin, Puck, and Tsai–Wu, and a micromechanics-based theory named MMF were applied to predict the static strength. A multiscale-based life prediction methodology called MMFatigue was used to predict and micromechanically explain the laminate S–N curves.

For the static strength, both the predictions and the experimental results show the same trend: the tensile strength increases as θ becomes shallower, while laminates with a shallow ply angle of 35° showed similar or even lower compressive strengths, especially for TA and TX laminates. One of the reasons for low compressive strengths of TA35 and TX35 is the transverse stress at the θ ply caused by the Poisson's effect.

In case of the fatigue life, the predicted S–N curves and the experimental results are in acceptable agreements. Compared with 45°, the shallow angles of 25° and 35° provide much longer laminate fatigue life for BX and TA laminates, while the shallow angle effects on the fatigue life becomes less for TA and TX. The effect of the shallow angle on the laminate fatigue life was explained using the constitutive effective stresses. For the BX laminates, the failure mode is either matrix or interface, and both interface and matrix effective stresses decrease as θ decreases. In case of the TA laminates, the volume fraction of the 0° ply is only 20% and the laminate failure is also dominated by the matrix and the interface at the θ ply. The effective stresses at the matrix and the interface decrease for a shallow angle causing the longest fatigue life. For the TX laminates, the volume fraction of the 0° ply is 50% and the laminate failure is mostly determined by the fibers at the 0° ply. A shallow ply angle provides a less fiber effective stress and consequently a longer TX fatigue life.

Declaration of Conflicting Interests

The author(s) declared no potential conflicts of interest with respect to the research, authorship, and/or publication of this article.

Funding

The author(s) received no financial support for the research, authorship, and/or publication of this article.

References

1. Veers PS, Ashwill TD, Sutherland HJ, et al. Trends in the design, manufacture and evaluation of wind turbine blades. *Wind Energy* 2003; 6: 245–259.

2. Griffin DA and Zuteck MD. Scaling of composite wind turbine blades for rotors of 80 to 120 meter diameter. *J Solar Energy Eng – Transact ASME* 2001; 123: 310–318.
3. Ha SK, Hayat K and Xu L. Effect of shallow-angled skins on the structural performance of the large-scale wind turbine blade. *Renew Energy* 2014; 71: 100–112.
4. Rotem A and Hashin Z. Fatigue failure of angle ply laminates. *AIAA J* 1976; 14: 868–872.
5. Kujawski D. Width effects on the tensile strength and fatigue behavior of angle-ply laminates. *Int J Fatigue* 1998; 20: 575–580.
6. Kawai M and Teranuma T. A multiaxial fatigue failure criterion based on the principal constant life diagrams for unidirectional carbon/epoxy laminates. *Compos Part A: Appl Sci Manuf* 2012; 43: 1252–1266.
7. Philippidis TP and Vassilopoulos AP. Fatigue of composite laminates under off-axis loading. *Int J Fatigue* 1999; 21: 253–262.
8. Tohgo K, Nakagawa S and Kageyama K. Fatigue behavior of CFRP cross-ply laminates under on-axis and off-axis cyclic loading. *Int J Fatigue* 2006; 28: 1254–1262.
9. Kawai M and Honda N. Off-axis fatigue behavior of a carbon/epoxy cross-ply laminate and predictions considering inelasticity and in situ strength of embedded plies. *Int J Fatigue* 2008; 30: 1743–1755.
10. Samborsky DD, Agastra P and Mandell JF. Fatigue trends for wind blade infusion resins and fabrics. AIAA SDM, Orlando, Wind Energy Session, 2010. AIAA-2010-2821..
11. Mandell JF, Samborsky DD, Agastra P, et al. Analysis of SNL/MSU/DOE fatigue database trends for wind turbine blade materials. Contractor Report SAND2010-7052, Sandia National Laboratories, Albuquerque, NM, 2010.
12. Tsai SW and Wu EM. A general theory of strength for anisotropic materials. *J Compos Mater* 1971; 5: 58–80.
13. Hashin Z. Failure criteria for unidirectional fiber composites. *J Appl Mech* 1980; 47: 329–334.
14. Puck A and Schürmann H. Failure analysis of FRP laminates by means of physically based phenomenological models. *Compos Sci Technol* 1998; 58: 1045–1067.
15. Philippidis TP and Passipoularidis VA. Residual strength after fatigue in composites: theory vs. experiment. *Int J Fatigue* 2007; 29: 2104–2116.
16. Kawai M and Koizumi M. Nonlinear constant life diagrams for carbon/epoxy laminates at room temperature. *Compos Part A: Appl Sci Manuf* 2007; 38: 2342–2353.
17. Kawai M, Matsuda Y and Yoshimura R. A general method for predicting temperature-dependent anisomorphic constant fatigue life diagram for a woven fabric carbon/epoxy laminate. *Compos Part A: Appl Sci Manuf* 2012; 43: 915–925.
18. Kawai M and Sagawa T. Temperature dependence of off-axis tensile creep rupture behavior of a unidirectional carbon/epoxy laminate. *Compos Part A: Appl Sci Manuf* 2008; 39: 523–539.
19. Kawai M and Murata T. A three-segment anisomorphic constant life diagram for the fatigue of symmetric angle-ply carbon/epoxy laminates at room temperature. *Compos Part A: Appl Sci Manuf* 2010; 41: 1498–1510.
20. Kawai M and Itoh N. A failure-mode based anisomorphic constant life diagram for a unidirectional carbon/epoxy laminate under off-axis fatigue loading at room temperature. *J Compos Mater* 2014; 48: 571–592.
21. Miyano Y, Nakada M, McMurray MK, et al. Prediction of flexural fatigue strength of CFRP composites under arbitrary frequency, stress ratio and temperature. *J Compos Mater* 1997; 31: 619–638.
22. Miyano Y, Nakada M, Kudoh H, et al. Prediction of tensile fatigue life for unidirectional CFRP. *J Compos Mater* 2000; 34: 538–550.
23. Miyano Y, Nakada M and Sekine N. Accelerated testing for long-term durability of FRP laminates for marine use. *J Compos Mater* 2005; 39: 5–20.
24. Miyano Y, Nakada M and Nishigaki K. Prediction of long-term fatigue life of quasi-isotropic CFRP laminates for aircraft use. *Int J Fatigue* 2006; 28: 1217–1225.
25. Kuraishi A. *Durability analysis of composite structures using the accelerated testing methodology*. PhD Thesis, Stanford University, USA, 2001.
26. Cai H, Miyano Y, Nakada M, et al. Long-term fatigue strength prediction of CFRP structure based on micromechanics of failure. *J Compos Mater* 2008; 42: 825–844.
27. Miyano Y, Nakada M and Cai H. Formulation of long-term creep and fatigue strengths of polymer composites based on accelerated testing methodology. *J Compos Mater* 2008; 42: 1897–1919.
28. Nakada M and Miyano Y. Formulation of time- and temperature-dependent strength of unidirectional carbon fiber reinforced plastics. *J Compos Mater* 2013; 47: 1897–1906.
29. Ha SK, Huang Y, Han HH, et al. Micromechanics of failure for ultimate strength predictions of composite laminates. *J Compos Mater* 2010; 44: 2347–2361.
30. Huang Y, Jin C and Ha SK. Strength prediction of triaxially loaded composites using a progressive damage model based on micromechanics of failure. *J Compos Mater* 2013; 47: 777–792.
31. Huang YC, Jin CZ and Ha SK. Micromechanics-based fatigue life prediction of composite materials. In: *First Brazilian conference on composite materials*, Natal-RN, Brazil, 16–19 June 2012, paper no. 211.
32. Huang YC. *Fatigue life prediction of composites*. PhD Thesis, Hanyang University, South Korea, 2014.
33. Abaqus version 6.11, http://www.simulia.com/.
34. Huang YC, Jin KK and Ha SK. Effects of fiber arrangement on mechanical behavior of unidirectional composites. *J Compos Mater* 2008; 42: 1851–1871.
35. Stassi-D'Alia F. Flow and fracture of materials according to a new limiting conditions of yielding. *Meccanica* 1967; 2: 178–195.
36. Theodore PP and Anastasios PV. Life prediction methodology for GFRP laminates under spectrum loading. *Compos A: Appl Sci Manuf* 2004; 35: 657–666.
37. Anastasios PV, Behzad DM and Thomas K. Influence of the constant life diagram formulation on the fatigue life prediction of composite materials. *Int J Fatigue* 2010; 32: 659–669.

38. Philippidis TP and Vassilopoulos AP. Fatigue of composite laminates under off-axis loading. *Int J Fatigue* 1999; 21: 253–262.
39. Shirazi AP and Varvani-Farahani A. A stiffness degradation based fatigue damage model for FRP composite of $(0/\theta)$ laminate systems. *Int J Fatigue* 2010; 17: 137–150.
40. ASTM D792. Standard test method for density and specific gravity of plastics by displacement.
41. ASTM D3039. Standard test method for tensile properties of polymer matrix composite materials.
42. ASTM D3410. Standard test method for compressive properties of polymer matrix composite materials with unsupported gage section by shear loading.
43. ASTM D3479. Standard test method for tension–tension fatigue of polymer matrix composite materials.
44. Camanho PP and Dávila CG. Mixed-mode decohesion finite elements for the simulation of delamination in composite materials. NASA-TM-2002-211737, 2002.
45. Kelly A and Tyson W. Tensile properties of fibre-reinforced metals: copper/tungsten and copper/molybdenum. *J Mech Phys Solid* 1965; 13: 329–350.
46. Hoppel CPR and De Teresa SJ. Effect of angle-ply orientation on compression strength of composite laminates. In: *15th U.S. Army symposium on solid mechanics*, Myrtle Beach, SC, 1999..

Appendix 1. Stress–strain curves of BX, TA, and TX

The tensile stress–strain curves and compressive stress–strain curves of BX, TA, and TX laminates are shown in Figures A1 and A2, respectively.

In order to verify the accuracy of the predictions, the tensile test of TA25 laminate and the compressive

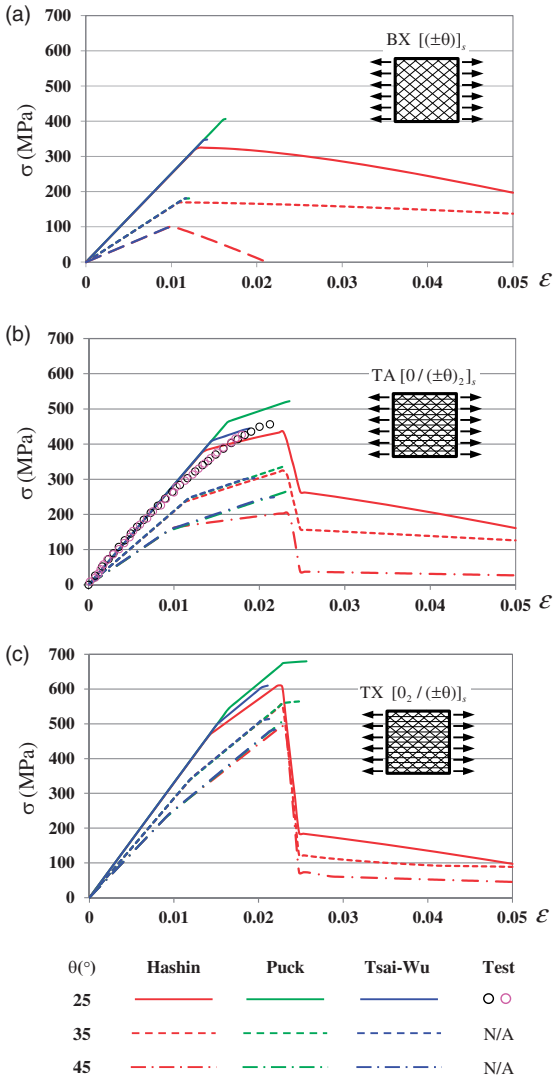

Figure A1. Tensile stress–strain curves: (a) BX, (b) TA, and (c) TX.

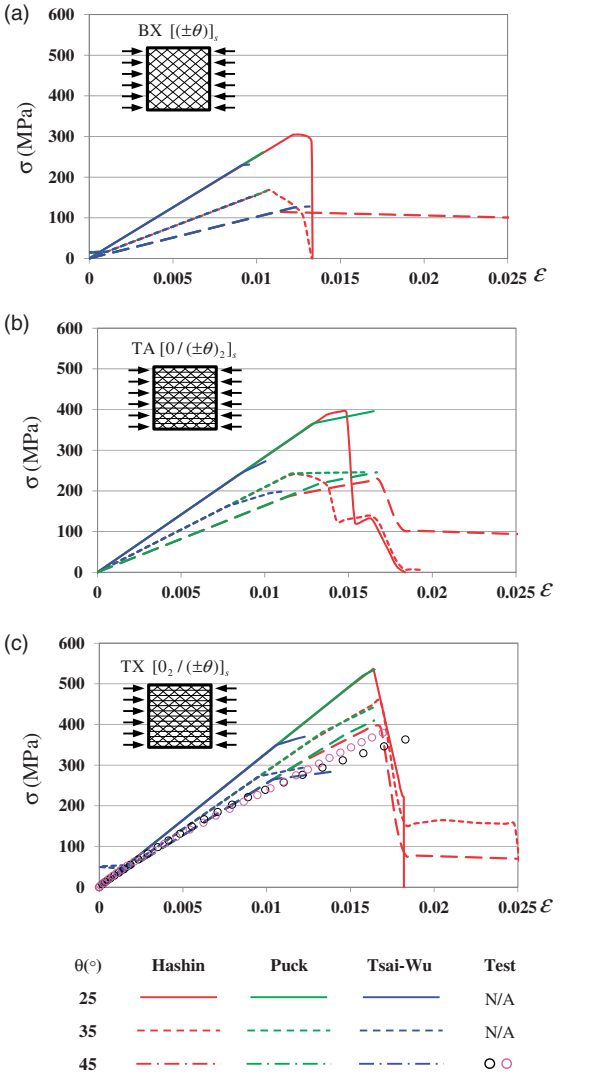

Figure A2. Compressive stress-strain curves: (a) BX, (b) TA, and (c) TX.

test of TX45 laminate were selected for stress–strain curves. The strains were measured using strain gauges. The stiffness of TA25 is 28.8 GPa from the test and is 28.4 GPa from the prediction using classical laminate theory (CLT), while for the TX45, the laminate test results give a stiffness of 25.6 GPa while CLT predicts 26.7 GPa. The average X_T of TA25 from the experiment is 452 MPa, while the predicted values are 435 MPa, 444 MPa, and 522 MPa based on the Hashin, Tsai–Wu, and Puck failure criteria, respectively. The test data give an average X_C of 381 MPa for TX45, while the Hashin, Tsai–Wu, and Puck failure criteria predict 395 MPa, 275 MPa, and 396 MPa for the X_C, respectively. Compared with the test data, the predicted stiffness and strength are in acceptable ranges.

Obviously, different failure criteria give different predictions of the static strengths. There is no general trend of the predicted strengths from different failure criteria. For example, the Tsai–Wu and Hashin failure criteria predict similar X_T, and the Puck criterion predicts the largest X_T. However, for the compressive case, the Puck and Hashin failure criteria predict similar X_C, and Tsai–Wu gives the lowest X_C out of the three criteria, which is in agreement with the trend found in Shirazi and Varvani-Farahani.[39]

The strength predictions based on FPF and LPF can also be observed from the stress–strain curves. For BX laminate, since there is only θ (or $-\theta$) ply, the strengths based on FPF and LPF are obviously the same. However, for TA and TX, after the FPF, the stiffnesses of failed plies are reduced, but other intact plies can still support the load, so the applied loading continues to increase up to the LPF.